universe

MDPI

Article

Analysis of the Geodesic Motions of Massive Particles in Kerr–Sen–AdS$_4$ Spacetime

Ziqiang Cai [1], Ming Liu [1], Wen-Qian Wang [1], Tong-Yu He [1], Zhan-Wen Han [1,2] and Rong-Jia Yang [1,3,4,5,*]

[1] College of Physics Science and Technology, Hebei University, Baoding 071002, China
[2] Yunnan Observatories, Chinese Academy of Sciences, Kunming 650216, China
[3] Hebei Key Lab of Optic-Electronic Information and Materials, Hebei University, Baoding 071002, China
[4] National-Local Joint Engineering Laboratory of New Energy Photoelectric Devices, Hebei University, Baoding 071002, China
[5] Key Laboratory of High-Pricision Computation and Application of Quantum Field Theory of Hebei Province, Hebei University, Baoding 071002, China
* Correspondence: yangrongjia@tsinghua.org.cn

Abstract: We consider geodesic motions in Kerr–Sen–AdS$_4$ spacetime. We obtain equations of motion for light rays and test particles. Using parametric diagrams, we show some regions where radial and latitudinal geodesic motions are allowed. We analyze the impact of parameters related to the dilatonic scalar on the orbit and find that it will result in more rich and complex orbital types.

Keywords: geodesic motion; ISCO; Kerr-Sen-AdS$_4$ black hole; orbit type

Citation: Cai, Z.; Liu, M.; Wang, W.-Q.; He, T.-Y.; Han, Z.-W.; Yang, R.-J. Analysis of the Geodesic Motions of Massive Particles in Kerr–Sen–AdS$_4$ Spacetime. *Universe* **2024**, *10*, 133. https://doi.org/10.3390/universe10030133

Academic Editor: Lorenzo Iorio

Received: 10 January 2024
Revised: 18 February 2024
Accepted: 21 February 2024
Published: 8 March 2024

1. Introduction

Studying test particles and light rays in spacetimes has been a matter of interest for a long time: it is an important channel for understanding black holes and predicts a number of observational effects. The study of geodesic motion can be traced back to the early work conducted by Hagihara [1], who analytically solved the equations of motion of test particles and light rays in Schwarzschild spacetime. It has been shown that the geodesic equations in Kerr, Reissner–Nordström, and Kerr–Newman spacetimes have the same mathematical structure [2]. Since then, many works in the literature have extensively investigated the equations of motion of particles and light rays in various spacetimes; see, for example, [3–8]. The geodesic equations in some spacetimes can be analytically solved in terms of the Weierstrass functions and the derivatives of Kleinian functions [4,6,9,10]. These methods have been applied to higher dimensional black holes [11–14], to Taub-NUT and wormhole spacetime [15,16], and to Kerr–Sen dilaton–axion black holes [9]. Recently, this analytical approach has been further developed and applied to the hyperelliptic case, where the analytical solutions of the equations of motion in the four-dimensional Schwarzschild–(A)dS, Reissner–Nordström(A)dS, and Kerr–(A)dS spacetimes were presented [6,11,17–20]. The motions of test particles were also studied in various black string spacetimes [21–27]. The radial time-like geodesic motion of the exterior nonextremal Kerr spacetime was classified in detail in [28]. Recently, Kerr geodesics in terms of Weierstrass elliptic functions were discussed in [29]. Other works (see, for example, refs. [28,30–46]) also discussed the possible geodesic motions in various spacetimes.

In ref. [47], a solution, including a nonzero negative cosmological constant for the Kerr–Sen solution, was obtained. Kerr–Sen–AdS$_4$ and Kerr–Newman–AdS$_4$ black holes have some similar properties, such as horizon geometry and conformal boundaries, but they exhibit some significant physical differences; for example, the former does not violate the reverse isoperimetric inequality, while the latter always strictly does. It is valuable to investigate particle motion in Kerr–Sen–AdS$_4$ spacetime, but analyses of the geodesic motions for massive particles in the Kerr–Sen–AdS$_4$ spacetime are still not presented. In

this paper, we will fill this gap. We will investigate in detail the geodesic motions in the background of the Kerr–Sen–AdS$_4$ black hole.

The order of this paper is as follows. In Section 2, we give a brief review of the Kerr–Sen–AdS$_4$ metric. In Section 3, we present the equations for geodesic motions in Kerr–Sen–AdS$_4$ spacetime. In Section 4, we give a full analysis of the geodesic equations. Finally, we will briefly summarize and discuss our results in Section 5.

2. The Kerr–Sen–AdS$_4$ Black Hole Solution

The Lagrangian including a nonzero negative cosmological constant in four-dimensional gauged Einstein–Maxwell dilaton–axion theory has the following form:

$$\mathcal{L}=\sqrt{-g}\left\{R-\frac{1}{2}(\partial\phi)^2-\frac{1}{2}e^{2\phi}(\partial\chi)^2-e^{-\phi}F^2+\frac{1}{l^2}\left[4+e^{-\phi}+e^{\phi}\left(1+\chi^2\right)\right]\right\}+\frac{\chi}{2}\varepsilon^{\mu\nu\rho\lambda}F_{\mu\nu}F_{\rho\lambda}, \tag{1}$$

where g is the determinant of the metric, R is the Ricci scalar, ϕ is the dilaton scalar field, $F_{\mu\nu}$ is the electromagnetic tensor, and $F^2=F_{\mu\nu}F^{\mu\nu}$, χ is the axion pseudoscalar field dual to the three-form antisymmetric tensor $H=-e^{2\phi}\star d\chi$ and $H^2=H_{\mu\nu\sigma}H^{\mu\nu\sigma}$, l is the cosmological scale, and $\varepsilon_{\mu\nu\rho\lambda}$ is the four-dimensional Levi–Civita antisymmetric tensor density. A solution for this Lagrangian, called the Kerr–Sen–AdS$_4$ black hole, was obtained in [47]. Written in terms of Boyer–Lindquist coordinates, it takes the following form:

$$\mathrm{d}s^2=-\frac{\Delta_r}{\rho^2}\left(\mathrm{d}t-\frac{a\sin^2\theta}{\Xi}d\varphi\right)^2+\frac{\rho^2}{\Delta_r}\mathrm{d}r^2+\frac{\rho^2}{\Delta_\theta}\mathrm{d}\theta^2+\frac{\Delta_\theta\sin^2\theta}{\rho^2}\left(a\mathrm{d}t-\frac{r^2+2br+a^2}{\Xi}\mathrm{d}\varphi\right)^2, \tag{2}$$

where

$$\Delta_r=\left(1+\frac{r^2+2br}{l^2}\right)\left(r^2+2br+a^2\right)-2Mr, \tag{3}$$

$$\Delta_\theta=1-\frac{a^2}{l^2}\cos^2\theta,\quad \Xi=1-\frac{a^2}{l^2},\quad \rho^2=r^2+2br+a^2\cos^2\theta, \tag{4}$$

in which $a=J/M$ is the angular momentum per unit mass of the black hole, $b=Q^2/2M$ is the dilatonic scalar charge, M is the mass of the black hole, and Q is the charge of the black hole. The horizons in metric (2) are given by $\Delta_r=0$. The horizons are local at $\Delta_r=0$, meaning that there could be up to four horizons, and one of them is probably a cosmological horizon. In addition, the four parameters in (2) may not be completely independent to avoid naked singularity; see, for example, if $M^2+b^2-2Mb-a^2<0$ for a zero cosmology constant, and Equation (2) presents a naked singularity spacetime. Here, we focus on exploring the case of Equation (2), representing a black hole.

For the convenience of discussion, we give contravariant metric components as follows:

$$\begin{aligned}
g^{tt}&=-\frac{(r^2+2br+a^2)^2\Delta_\theta\sin^2\theta-a^2-a^2\Delta_r\sin^4\theta}{\rho^2\Delta_\theta\Delta_r\sin^2\theta},\\
g^{rr}&=\frac{\Delta_r}{\rho^2},\\
g^{\theta\theta}&=\frac{\Delta_\theta}{\rho^2},\\
g^{\varphi\varphi}&=-\frac{(a^2\Delta_\theta\sin^2\theta-\Delta_r)\Xi^2}{\rho^2\Delta_\theta\Delta_r\sin^2\theta},\\
g^{t\varphi}&=g^{\varphi t}=\frac{(a\Delta_r\sin^2\theta-a\Delta_\theta(r^2+2br+a^2)\sin^2\theta)\Xi}{\rho^2\Delta_\theta\Delta_r\sin^2\theta}.
\end{aligned} \tag{5}$$

The Kerr–Sen–AdS$_4$ black hole (2) reduces to the Kerr–AdS$_4$ solution [48,49] for $b = 0$ and reduces to the Kerr–Sen solution [50] when l tends to infinity.

3. The Geodesic Equations

In this section, we will derive the equations of motion for massive particles, the background of Kerr–Sen–AdS$_4$ black holes (2), by using the Hamilton–Jacobi formalism, and later we will introduce effective potentials for the r and θ motion. The Hamilton–Jacobi equation is

$$\frac{\partial S}{\partial \tau} + \frac{1}{2} g^{ij} \frac{\partial S}{\partial x^i} \frac{\partial S}{\partial x^j} = 0, \tag{6}$$

which can be solved with an ansatz for the action

$$S = \frac{1}{2}\tau - Et + L_z \phi + S_\theta(\theta) + S_r(r). \tag{7}$$

where τ is an affine parameter along the geodesic. The energy E and the angular momentum L, two constants of motion, are related to the the generalized momenta P_t and P_ϕ as

$$P_t = g_{tt}\dot{t} + g_{t\varphi}\dot{\varphi} = -E, \quad P_\phi = g_{\varphi\varphi}\dot{\varphi} + g_{t\varphi}\dot{t} = L, \tag{8}$$

where the dot denotes the derivative with respect to τ. Since $g_{t\varphi}$ depends on b, this parameter will affect the energy E and the angular momentum L of the test particle compared with the case in the Kerr–AdS$_4$ solution [6,18]. Using Equations (6)–(8), we have

$$\begin{aligned} &\Delta_\theta \left(\frac{\partial S}{\partial \theta}\right)^2 + a^2 \cos^2\theta - \frac{2aEL\Xi - E^2 a^2 \sin^2\theta}{\Delta_\theta} + \frac{L^2\Xi^2}{\Delta_\theta \sin^2\theta} \\ &= -\Delta_r \left(\frac{\partial S}{\partial r}\right)^2 - \left(r^2 + 2br\right) + \frac{\left(r^2 + 2br + a^2\right)^2 E^2 + a^2 L^2 \Xi^2 - 2a\left(r^2 + 2br + a^2\right) EL\Xi}{\Delta_r}. \end{aligned} \tag{9}$$

The left-hand side of Equation (9) depends only on θ, and the right-hand side depends only on r. With the ansatz Equation (7) and the Carter constant [51], we obtain the equations of motion for massive particles:

$$\rho^4 \left(\frac{\mathrm{d}r}{\mathrm{d}\tau}\right)^2 = -\Delta_r \left[K + \left(r^2 + 2br\right)\right] + \left[\left(r^2 + 2br + a^2\right)E - aL\Xi\right]^2, \tag{10}$$

$$\rho^4 \left(\frac{\mathrm{d}\theta}{\mathrm{d}\tau}\right)^2 = \Delta_\theta \left(K - a^2 \cos^2\theta\right) - \frac{1}{\sin^2\theta}\left(aE\sin^2\theta - L\Xi\right)^2, \tag{11}$$

$$\rho^2 \left(\frac{\mathrm{d}\varphi}{\mathrm{d}\tau}\right) = \frac{a\left(r^2 + 2br + a^2\right)E\Xi - a^2 L\Xi^2}{\Delta_r} - \frac{1}{\Delta_\theta \sin^2\theta}\left(aE\Xi\sin^2\theta - L\Xi^2\right), \tag{12}$$

$$\rho^2 \left(\frac{\mathrm{d}t}{\mathrm{d}\tau}\right) = \frac{E\left(r^2 + 2br + a^2\right)^2 - a\left(r^2 + 2br + a^2\right)L\Xi}{\Delta_r} - \frac{\sin^2\theta}{\Delta_\theta}\left(a^2 E - \frac{aL\Xi}{\sin^2\theta}\right), \tag{13}$$

where K is the Carter constant [51]. From Equation (11), we have a bound on the Carter constant: $K \geq (aE - L\Xi)^2$. Bounds on the Carter constant for Kerr black holes were first discussed in [51,52], and stronger bounds on the Carter constant for Kerr black holes were discussed in detail in [28].

From Equations (10) and (11), we introduce two effective potentials, V_{reff} and $V_{\theta eff}$, such that $V_{reff} = E$ and $V_{\theta eff} = E$, corresponding to $\left(\frac{\mathrm{d}r}{\mathrm{d}\tau}\right)^2 = 0$ and $\left(\frac{\mathrm{d}\theta}{\mathrm{d}\tau}\right)^2 = 0$, respectively,

$$V_{reff} = \frac{aL\Xi \pm \sqrt{\Delta_r[K + (r^2 + 2br)]}}{r^2 + 2br + a^2}, \tag{14}$$

$$V_{\theta eff} = \frac{L\Xi \pm \sqrt{\Delta_\theta (K - a^2\cos^2\theta)\sin^2\theta}}{a\sin^2\theta}. \tag{15}$$

V_{reff} is finite at $r = 0$ due to the presence of a; however, if $r = -b \pm \sqrt{b^2 - a^2}$, it will diverge. $V_{\theta eff}$ is finite for $\theta = \pi/2$, while it will diverge for $\theta = 0$. To simplify the equations of motion, we adopt the Mino time λ [53] connected to the proper time τ via $\frac{\mathrm{d}\tau}{\mathrm{d}\lambda} = \rho^2$, and then the equations of motions can be rewritten as

$$\left(\frac{\mathrm{d}r}{\mathrm{d}\lambda}\right)^2 = -\Delta_r\left(K + r^2 + 2br\right) + \left[\left(r^2 + 2br + a^2\right)E - aL\Xi\right]^2, \tag{16}$$

$$\left(\frac{\mathrm{d}\theta}{\mathrm{d}\lambda}\right)^2 = \Delta_\theta\left(K - a^2\cos^2\theta\right) - \frac{1}{\sin^2\theta}\left(aE\sin^2\theta - L\Xi\right)^2, \tag{17}$$

$$\frac{\mathrm{d}\varphi}{\mathrm{d}\lambda} = \frac{a\left(r^2 + 2br + a^2\right)E\Xi - a^2L\Xi^2}{\Delta_r} - \frac{1}{\Delta_\theta\sin^2\theta}\left(aE\Xi\sin^2\theta - L\Xi^2\right), \tag{18}$$

$$\frac{\mathrm{d}t}{\mathrm{d}\lambda} = \frac{E\left(r^2 + 2br + a^2\right)^2 - a\left(r^2 + 2br + a^2\right)L\Xi}{\Delta_r} - \frac{\sin^2\theta}{\Delta_\theta}\left(a^2E - \frac{aL\Xi}{\sin^2\theta}\right). \tag{19}$$

Introducing some dimensionless quantities to rescale the parameters

$$\tilde{r} = \frac{r}{M},\ \tilde{a} = \frac{a}{M},\ \tilde{t} = \frac{t}{M},\ \tilde{L} = \frac{L}{M},\ \tilde{l} = \frac{l}{M},\ \tilde{b} = \frac{b}{M},\ \tilde{K} = \frac{K}{M^2},\ \gamma = M\lambda, \tag{20}$$

then the equations of motion (16)–(19) can be formulated as

$$\left(\frac{\mathrm{d}\tilde{r}}{\mathrm{d}\gamma}\right)^2 = -\Delta_{\tilde{r}}\left(\tilde{K} + \tilde{r}^2 + 2\tilde{b}\tilde{r}\right) + \left[\left(\tilde{r}^2 + 2\tilde{b}\tilde{r} + \tilde{a}^2\right)E - \tilde{a}\tilde{L}\Xi\right]^2 \equiv \tilde{R}(\tilde{r}), \tag{21}$$

$$\left(\frac{\mathrm{d}\theta}{\mathrm{d}\gamma}\right)^2 = \Delta_\theta\left(\tilde{K} - \tilde{a}^2\cos^2\theta\right) - \frac{1}{\sin^2\theta}\left(\tilde{a}E\sin^2\theta - \tilde{L}\Xi\right)^2 \equiv \tilde{\Theta}(\theta), \tag{22}$$

$$\frac{\mathrm{d}\varphi}{\mathrm{d}\gamma} = \frac{\tilde{a}\left(\tilde{r}^2 + 2\tilde{b}\tilde{r} + \tilde{a}^2\right)E\Xi - \tilde{a}^2\tilde{L}\Xi^2}{\Delta_{\tilde{r}}} - \frac{1}{\Delta_\theta\sin^2\theta}\left(\tilde{a}E\Xi\sin^2\theta - \tilde{L}\Xi^2\right), \tag{23}$$

$$\frac{\mathrm{d}\tilde{t}}{\mathrm{d}\gamma} = \frac{E\left(\tilde{r}^2 + 2\tilde{b}\tilde{r} + \tilde{a}^2\right)^2 - \tilde{a}\left(\tilde{r}^2 + 2\tilde{b}\tilde{r} + \tilde{a}^2\right)\tilde{L}\Xi}{\Delta_{\tilde{r}}} - \frac{\sin^2\theta}{\Delta_\theta}\left(\tilde{a}^2E - \frac{\tilde{a}\tilde{L}\Xi}{\sin^2\theta}\right), \tag{24}$$

where

$$\Delta_\theta = 1 - \frac{\tilde{a}^2}{\tilde{l}^2}\cos^2\theta = 1 - \frac{a^2}{l^2}\cos^2\theta, \quad \Delta_{\tilde{r}} = \left(1 + \frac{\tilde{r}^2 + 2\tilde{b}\tilde{r}}{\tilde{l}^2}\right)\left(\tilde{r}^2 + 2\tilde{b}\tilde{r} + \tilde{a}^2\right) - 2\tilde{r}. \tag{25}$$

And the effective potentials can be expressed in terms of a dimensionless quantity as

$$\tilde{V}_{reff} = \frac{\tilde{a}\tilde{L}\Xi \pm \sqrt{\Delta_{\tilde{r}}\left(\tilde{K} + \tilde{r}^2 + 2\tilde{b}\tilde{r}\right)}}{\tilde{r}^2 + 2\tilde{b}\tilde{r} + \tilde{a}^2}, \tag{26}$$

$$\tilde{V}_{\theta eff} = \frac{\tilde{L}\Xi \pm \sqrt{\Delta_\theta\left(\tilde{K} - \tilde{a}^2\cos^2\theta\right)\sin^2\theta}}{\tilde{a}\sin^2\theta}. \tag{27}$$

4. Analysis of the Geodesic Equations

In this section, we will give a full analysis of the geodesic equations of motion in the Kerr–Sen–AdS$_4$ spacetime and investigate the possible orbit types.

In ref. [6], two theorems were proved for the case of the Kerr–AdS$_4$ solution. We find those two theorems still holds for the Kerr–Sen–AdS$_4$ solution (2), though the parameter b will change the values of the Carter constant $\tilde{K}$, the energy $\tilde{E}$, and the angular momentum $\tilde{L}$:

Theorem 1. *The modified Carter constant* $\tilde{Q} \equiv \tilde{K} - \left(\tilde{a}E - \tilde{L}\Xi\right)^2$ *is zero if a geodesic lies entirely in the equatorial plane* $\theta = \pi/2$ *or if it hits the ring singularity* $\rho = 0$.

Proof. For a geodesic that lies entirely in the equatorial plane, one has $\theta(\gamma) = \pi/2$ for all γ, implying that $(\Theta(\theta) = d\theta/d\gamma)^2 = 0$, which gives

$$0 = \tilde{\Theta}\Big(\theta = \frac{\pi}{2}\Big) = \tilde{K} - \left(\tilde{a}E - \tilde{L}\Xi\right)^2 \equiv \tilde{Q}. \tag{28}$$

If a geodesic hits the ring singularity, there is a γ such that $\tilde{r}(\gamma) = 0$ and $\theta(\gamma) = \pi/2$. Since $\tilde{R}(\tilde{r}) \geq 0$ and $\tilde{\Theta}(\theta) \geq 0$ for all γ and θ, in particular for $\tilde{r} = 0$ and $\theta = \pi/2$, it follows

$$0 \leq \tilde{R}(0) = -\tilde{a}^2\left[\tilde{K} - \left(\tilde{a}E - \tilde{L}\Xi\right)^2\right] = -\tilde{a}^2\tilde{Q} \Rightarrow \tilde{Q} \leq 0. \tag{29}$$

And as above, $\tilde{\Theta}(\pi/2) = \tilde{Q} \geq 0$. Combining these two results yields $\tilde{Q} = 0$. □

Theorem 2. *All time-like and null geodesics have* $\tilde{K} \geq 0$ *if* $1 > \tilde{a}^2/\tilde{l}^2$. *In this case,* $\tilde{K} = 0$ *implies* $\tilde{Q} = 0$ *and the geodesic lies entirely in the equatorial plane.*

Proof. A geodesic can only exist if there are values for $\tilde{r}(\gamma)$ with $\tilde{R}(\tilde{r}) \geq 0$ and $\theta(\gamma)$ with $\Theta(\tilde{\theta}) \geq 0$. From $1 > \tilde{a}^2/\tilde{l}^2$, one has $\Delta_\theta = 1 - \frac{\tilde{a}^2}{\tilde{l}^2}\cos^2\theta > 1 - \cos^2\theta \geq 0$. If $\tilde{K} < 0$, then

$$\tilde{\Theta}(\theta) \equiv \Delta_\theta\Big(\tilde{K} - \tilde{a}^2\cos^2\theta\Big) - \frac{1}{\sin^2\theta}\Big(\tilde{a}E\sin^2\theta - \tilde{L}\Xi\Big)^2 \leq 0 \tag{30}$$

for all values of θ. If now $\tilde{K} = 0$, consequently

$$\tilde{\Theta}(\theta) = -\Delta_\theta\tilde{a}^2\cos^2\theta - \frac{1}{\sin^2\theta}\Big(\tilde{a}E\sin^2\theta - \tilde{L}\Xi\Big)^2 \leq 0. \tag{31}$$

$\tilde{\Theta}(\theta) = 0$ only if $\cos^2\theta = 0$ and additionally $\tilde{a}E\sin^2\theta - \tilde{L}\Xi = \tilde{a}E - \tilde{L}\Xi = 0$. □

From these two theorems, it is obvious that the modified Carter constant $\tilde{Q}$ has a geometric interpretation since it is related to possible θ values of the orbits. These two theorems will be useful in the study of geodesic motion in the background of a rotating black hole.

Types of Latitudinal Motion

First we consider the function $\tilde{\Theta}(\theta)$ in Equation (22) for massive particle. Let $v = \cos^2\theta$ with $v \in [0, 1]$; the function $\tilde{\Theta}$ can be written as

$$\tilde{\Theta}(v) = \left(1 - \frac{\tilde{a}^2}{\tilde{l}^2}v\right)\left(\tilde{K} - \tilde{a}^2 v\right) - \frac{1}{1-v}\left[\tilde{a}E(1-v) - \tilde{L}\Xi\right]^2. \tag{32}$$

Geodesic motion is possible only for $\tilde{\Theta}(v) \geq 0$, which also implies that $\tilde{K} \geq 0$ in all spacetimes with $1 > \tilde{a}^2/\tilde{l}^2$. The zeros of $\tilde{\Theta}(\theta)$ are the turning points of the latitudinal motion. Assuming that $\tilde{\Theta}(v)$ has some zeros in $[0, 1]$, the number of zeros changes only if (i) a zero crosses 0 or 1 or (ii) a double or triple zero occurs. If $v = 0$ is a zero, then

$$\tilde{\Theta}(v=0) = \tilde{K} - \left(\tilde{a}E - \tilde{L}\Xi\right)^2, \tag{33}$$

or

$$\tilde{L} = \frac{\tilde{a}E \pm \sqrt{\tilde{K}}}{\Xi}. \tag{34}$$

From Equation (32), we see that $v = 1$ is a pole of $\tilde{\Theta}(v)$ for $\tilde{L} \neq 0$. So $v = 1$ is a zero of $\tilde{\Theta}(v)$ only if $\tilde{L} = 0$; therefore, we have

$$\tilde{\Theta}(v=1, \tilde{L}=0) = \left(1 - \frac{\tilde{a}^2}{\tilde{l}^2}\right)\left(\tilde{K} - \tilde{a}^2\right). \tag{35}$$

So for $\tilde{\Theta}(v=1, \tilde{L}=0) = 0$, we have $\tilde{K} = \tilde{a}^2$. In order to remove the pole of $\tilde{\Theta}(v)$ at $v = 1$, we consider another function

$$\tilde{\Theta}'(v) = (1-v)\left(1 - \frac{\tilde{a}^2}{\tilde{l}^2}v\right)\left(\tilde{K} - \varepsilon\tilde{a}^2 v\right) - \left[\tilde{a}E(1-v) - \tilde{L}\Xi\right]^2, \tag{36}$$

where $\tilde{\Theta}(v) = \frac{1}{1-v}\tilde{\Theta}'(v)$. The double zeros satisfy the following conditions,

$$\tilde{\Theta}'(v) = 0 \qquad \text{and} \qquad \frac{\mathrm{d}\tilde{\Theta}'(v)}{\mathrm{d}v} = 0, \tag{37}$$

which implies

$$\tilde{L} = \frac{\left(6E \pm \sqrt{36E^2 - \frac{36}{\tilde{l}^2}\tilde{K}}\right)\left(-\frac{12}{\tilde{l}^2}\tilde{a}^2 + 12\right)}{-\frac{144}{\tilde{l}^2}\tilde{a}\Xi}. \tag{38}$$

We can use this information to analyze the θ motion of all possible geodesics for given parameters of the black hole, $\tilde{a}$, $\tilde{b}$, and $\tilde{l}$. We see that Equation (32) does not depend obviously on the parameter $\tilde{b}$, but it will change the number of zeros or the positions of the zeros via changing the Carter constant $\tilde{K}$, the energy $\tilde{E}$ and the angular momentum $\tilde{L}$ compared with the case for the Kerr–AdS$_4$ solution in Einstein's gravity [6,18] or the case for the Kerr–AdS$_4$ solution with $q = 0$ in $f(R)$ gravity [4].

We plot parametric $\tilde{L} - E^2$ diagrams in Figure 1 from the condition of $v = 0$ being a zero (Equation (34)) and the condition of double zeros (Equation (38)). The half plane is divided into four regions by the curves. The boundaries of region a are given by $\tilde{L} = \frac{\tilde{a}E \pm \sqrt{\tilde{K}}}{\Xi}$, which will get lager if $\tilde{K}$ grows, or it will shift up or down if $\tilde{a}$ changes. In regions a and b, geodesic motions are possible because in all other regions $\Theta(v)$ is negative for all $v \in (0,1)$. The function $\tilde{\Theta}$ has a single zero in region a, where the geodesics will cross the equatorial plane ($\tilde{K} > (\tilde{a}E - \tilde{L}\Xi)^2$ or $\tilde{Q} > 0$). In region b, the function $\tilde{\Theta}$ has two zeros, corresponding to motion above or below the equatorial plane ($\tilde{K} < (\tilde{a}E - \tilde{L}\Xi)^2$ or $\tilde{Q} < 0$). If $\tilde{K} = (\tilde{a}E - \tilde{L}\Xi)^2$, according to the Theorem 1, the geodesics will remain in the equatorial plane.

We note that Equation (36) may have triple zeros which satisfy the following conditions:

$$\tilde{\Theta}'(v) = 0, \qquad \frac{\mathrm{d}\tilde{\Theta}'(v)}{\mathrm{d}v} = 0, \qquad \text{and} \qquad \frac{\mathrm{d}\tilde{\Theta}'^2(v)}{\mathrm{d}v^2} = 0. \tag{39}$$

In Figure 2, we plot the $\tilde{L} - E$ diagram for the triple root of function $\tilde{\Theta}$ with some special values of parameters. We observe that $\tilde{L}$ has two branches: the inferior branches decrease as E increases and run close to zero, while the upper branches increase as E increases.

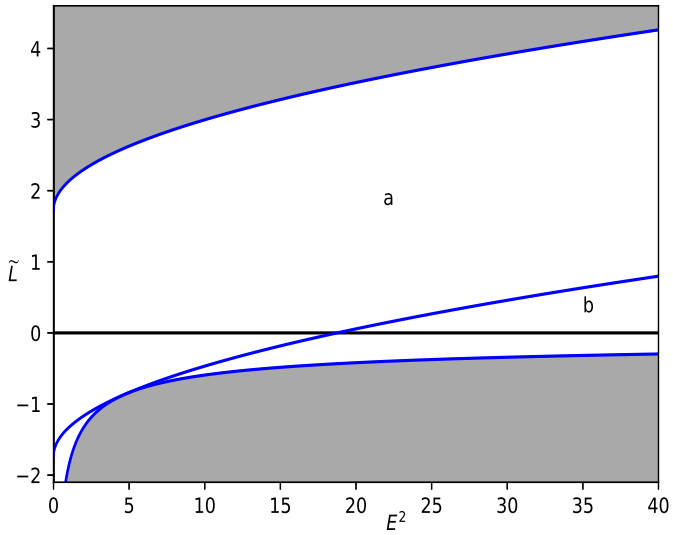

Figure 1. Parametric $\tilde{L} - E^2$-diagram for the function $\tilde{\Theta}$ with $\tilde{a} = 0.4, \tilde{K} = 3, \tilde{l}^2 = 3 \times 10^5$. $\tilde{\Theta}$ possesses one zero in region a and two zeros in region b. In the grey areas, geodesic motion is not allowed.

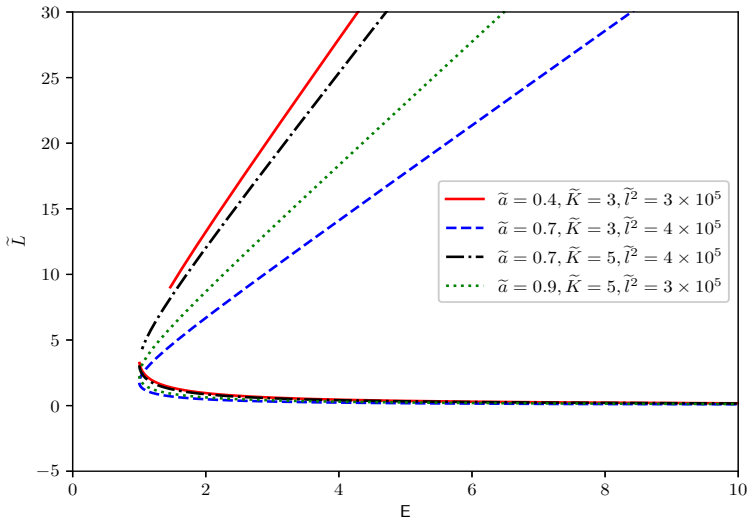

Figure 2. Parametric $\tilde{L} - E$ diagram for the triple root of function $\tilde{\Theta}$ with some special values of parameters.

5. Analysis of the Radial Geodesic Equations

In this section, we will give a full analysis of the radial geodesic equations of motion in the background of Kerr–Sen–AdS$_4$ black holes and investigate the possible types of orbit, the equatorial circular orbits, and the innermost stable circular orbits for massive particles.

5.1. Types of Radial Motion

For massive particles, a radial geodesic motion is possible if $\tilde{R}(\tilde{r}) \geq 0$. The zeros of the function $\tilde{R}$ in Equation (21) are the turning points of orbits of particles, so $\tilde{R}(\tilde{r}) = 0$ determines the possible types of orbits. Since the polynomial $\tilde{R}(\tilde{r})$ is of degree six in $\tilde{r}$ for massive particles, see that, for example, the expansion of $\tilde{R}(\tilde{r})$ takes the form

$$\tilde{R}(\tilde{r}) = f_0 + f_1\tilde{r} + \cdots + f_6\tilde{r}^6, \tag{40}$$

where

$$f_0 = E^2\tilde{a}^4 - 2E\Xi\tilde{a}^3\tilde{L} - \tilde{a}^2\tilde{K} + \Xi^2\tilde{a}^2\tilde{L}^2, \quad (41)$$

$$f_1 = 4E^2\tilde{a}^2\tilde{b} - 4E\Xi\tilde{a}\tilde{b}\tilde{L} - \frac{2\tilde{a}^2\tilde{b}\tilde{K}}{\tilde{l}^2} - 2\tilde{a}^2\tilde{b} - 2\tilde{b}\tilde{K} + 2\tilde{K}, \quad (42)$$

$$f_2 = -\frac{4\tilde{a}^2\tilde{b}^2}{\tilde{l}^2} + 2E^2\tilde{a}^2 - 2E\Xi\tilde{a}\tilde{L} - \frac{\tilde{a}^2\tilde{K}}{\tilde{l}^2} - \tilde{a}^2 + 4E^2\tilde{b}^2 - \frac{4\tilde{b}^2\tilde{K}}{\tilde{l}^2} - 4\tilde{b}^2 + 4\tilde{b} - \tilde{K}, \quad (43)$$

$$f_3 = -\frac{4\tilde{a}^2\tilde{b}}{\tilde{l}^2} + 4E^2\tilde{b} - \frac{4\tilde{b}\tilde{K}}{\tilde{l}^2} - \frac{8\tilde{b}^3}{\tilde{l}^2} - 4\tilde{b} + 2, \quad (44)$$

$$f_4 = -\frac{\tilde{a}^2}{\tilde{l}^2} - \frac{12\tilde{b}^2}{\tilde{l}^2} + E^2 - \frac{\tilde{K}}{\tilde{l}^2} - 1, \quad (45)$$

$$f_5 = -\frac{6\tilde{b}}{\tilde{l}^2}, \quad (46)$$

$$f_6 = -\frac{1}{\tilde{l}^2}, \quad (47)$$

so it has, in general, six possibly complex zeros of which the real zeros are of interest for the type of motion. The parameter $\tilde{b}$ will change the number of zeros or the positions of the zeros for other parameters taking the same values in the Kerr–AdS$_4$ case [6,18]. If $\tilde{r} = 0$ is an allowed value of $\tilde{r}(\gamma)$, we have

$$0 \leq \tilde{R}(0) = -\tilde{a}^2\left[\tilde{K} - \left(\tilde{a}E - \tilde{L}\Xi\right)^2\right] = -\tilde{a}^2\tilde{Q}. \quad (48)$$

Therefore, $\tilde{r} = 0$ can only be crossed if $\tilde{Q} \leq 0$, which corresponds to region b of the θ motion. Since $\tilde{Q} > 0$ in region a of the θ motion, a transition from positive to negative $\tilde{r}$ is not possible. The number of real zeros of $\tilde{R}$ changes if a double zero occurs:

$$\tilde{R}(\tilde{r}) = 0 \qquad \text{and} \qquad \frac{\mathrm{d}\tilde{R}(\tilde{r})}{\mathrm{d}\tilde{r}} = 0. \quad (49)$$

When the number of real zeros $\tilde{R}$ changes, the type of orbit will change.

Now, we discuss the possible types of orbit on which $\tilde{R}(\tilde{r}) \geq 0$. The types of orbit were discussed in detail in [4,6]. For the sake of discussion, we consider a black hole with two horizons to illustrate this point. Let r_1 and r_2 denote the roots of $\tilde{R}(\tilde{r})$, let $\tilde{r}_+$ be the outer event horizon, and let $\tilde{r}_-$ be the inner event horizon.

1. Transit orbit (TrO): $-\infty < \tilde{r} < \infty$. The particle starts from $\pm\infty$ and goes to $\mp\infty$.

2. Escape orbit (EO): $r_1 \leq \tilde{r} < \infty$ with $r_1 > \tilde{r}_+$, or $-\infty < \tilde{r} \leq r_1$ with $r_1 < \tilde{r}_-$. The particle approaches the black hole but turns around at a certain point to escape towards infinity.

3. Two-world escape orbit (TEO): $r_1 \leq \tilde{r} < \infty$ with $r_1 < \tilde{r}_-$, or $-\infty < \tilde{r} \leq r_1$ with $r_1 > \tilde{r}_+$. The particle crosses the horizon twice and can enter another universe.

4. Crossover one-world escape orbit (COEO): $\tilde{r}_- < r_1 < \tilde{r}_+$ with $r_1 \leq \tilde{r} < \infty$ or $-\infty < \tilde{r} \leq r_1$. The particle crosses the outer horizon or inner horizon and can enter another universe.

5. Bound orbit (BO): $r_1 \leq \tilde{r} \leq r_2$ with $r_1, r_2 > \tilde{r}_+$ or $r_1, r_2 < \tilde{r}_-$ or $\tilde{r}_- < r_1, r_2 < \tilde{r}_+$. The particle oscillates between r_1 and r_2.

6. Crossover one-world bound orbit (COBO): $r_1 \leq \tilde{r} \leq r_2$ with $r_1 < \tilde{r}_-$ and $\tilde{r}_- < r_2 < \tilde{r}_+$, or $r_1 \leq \tilde{r} \leq r_2$ with $\tilde{r}_- < r_1 < \tilde{r}_+$ and $r_2 > \tilde{r}_+$. The particle oscillates between r_1 and r_2 and crosses the inner or outer horizon.

7. Many-world bound orbit (MBO): $r_1 \leq \tilde{r} \leq r_2$ with $r_2 > \tilde{r}_+$ and $r_1 < \tilde{r}_-$. The particle crosses the horizon multiple times and can enter another universe.

8. Circular orbit (CO): $\tilde{R}(\tilde{r})$ has real double roots. The particle circles around the black hole with $r_1 = r_2 \geq \tilde{r}_+$ (COO), when $r_1 = r_2 = \tilde{r}_+$, the orbits are confined at the even event horizon. The particle circles outside the inner horizon with $r_1 = r_2 < \tilde{r}_-$ (COI), when

$r_1 = r_2 = \tilde{r}_-$, the orbits are confined at the even inner horizon. The particle circles in the black hole with $\tilde{r}_- < r_1 = r_2 < \tilde{r}_+$ (COIn).

In the following, we will discuss in detail the types of orbit for the radial geodesic motion of massive particles.

First, we discuss in detail two cases: $\tilde{R}(\tilde{r})$ has no real zero or has two real zeros. Other cases can be discussed similarly but are much more complex. Because the more zeros there are, the more types of orbits there are.

Region I: $\tilde{R}$ has no real zero. If $\tilde{Q} < 0$, we have $\tilde{R}(\tilde{r}) > 0$ with $\tilde{r} \in (-\infty, +\infty)$, orbit type: TrO. If $\tilde{Q} = 0$, we have $\tilde{r} \in [0, +\infty)$, orbit type: TEO.

Region II: $\tilde{R}$ has two real zeros. There are two cases needed to consider: these two zeros are a double zero or they are not.

Case A: these two zeros are not a double zero.

(1) If $\tilde{Q} \geq 0$: (a) $r_1 \leq \tilde{r} \leq r_2$ with $r_1, r_2 > \tilde{r}_+$ or $r_1, r_2 < \tilde{r}_-$ or $\tilde{r}_- < r_1, r_2 < \tilde{r}_+$, orbit type: BO; (b) $r_1 \leq \tilde{r} \leq r_2$ with $r_1 < \tilde{r}_-$ and $\tilde{r}_- < r_2 < \tilde{r}_+$, or with $\tilde{r}_- < r_1 < \tilde{r}_+$ and $r_2 > \tilde{r}_+$, orbit type: COBO; (c) $r_1 \leq \tilde{r} \leq r_2$ with $r_2 > \tilde{r}_+$ and $r_1 < \tilde{r}_-$, orbit type: MBO; (d) $\tilde{r} \leq r_1$ with $r_1 < 0$ or $\tilde{r} \geq r_2$ with $r_2 < \tilde{r}_-$, orbit type: EO or TEO; (e) $\tilde{r} \leq r_1$ with $r_1 < 0$ or $\tilde{r} \geq r_2$ with $\tilde{r}_- < r_2 < \tilde{r}_+$, orbit type: EO or COEO; (f) $\tilde{r} \leq r_1$ with $r_1 < 0$ or $\tilde{r} \geq r_2$ with $r_2 > \tilde{r}_+$, orbit type: EO.

(2) If $\tilde{Q} \leq 0$: (a) $r_1 \leq \tilde{r} \leq r_2$ with $r_1 \leq 0$ and $r_2 < \tilde{r}_-$, orbit type: BO; (b) $r_1 \leq \tilde{r} \leq r_2$ with $r_1 \leq 0$ and $\tilde{r}_- < r_2 < \tilde{r}_+$, orbit type: COBO; (c) $r_1 \leq \tilde{r} \leq r_2$ with $r_2 > \tilde{r}_+$ and $r_1 \leq 0$, orbit type: MBO; (d) $\tilde{r} \leq r_1$ or $\tilde{r} \geq r_2$ with $r_1 < r_2 < 0$, orbit type: EO or TEO; (e) $\tilde{r} \leq r_1$ or $\tilde{r} \geq r_2$ with $0 \leq r_1 < r_2 < \tilde{r}_-$, orbit type: EO or TEO; (f) $\tilde{r} \leq r_1$ or $\tilde{r} \geq r_2$ with $0 \leq r_1 < \tilde{r}_- < r_2 < \tilde{r}_+$, orbit type: EO or COEO; (g) $\tilde{r} \leq r_1$ or $\tilde{r} \geq r_2$ with $\tilde{r}_- < r_1 < r_2 < \tilde{r}_+$, orbit type: COEO; (h) $\tilde{r} \leq r_1$ or $\tilde{r} \geq r_2$ with $0 \leq r_1 < \tilde{r}_- < \tilde{r}_+ < r_2$, orbit type: EO; (i) $\tilde{r} \leq r_1$ or $\tilde{r} \geq r_2$ with $\tilde{r}_- < r_1 < \tilde{r}_+ < r_2$, orbit type: COEO or EO; (j) $\tilde{r} \leq r_1$ or $\tilde{r} \geq r_2$ with $\tilde{r}_+ < r_1 < r_2$, orbit type: TEO or EO.

Case B: those two zeros are a double zero.

If $r_1 = r_2 > \tilde{r}_+$, orbit type: COO; if $r_1 = r_2 < \tilde{r}_-$, orbit type: COI; if $\tilde{r}_- < r_1 = r_2 < \tilde{r}_+$, orbit type: COIn.

Region III: $\tilde{R}$ has four real zeros and $\tilde{R}(\tilde{r}) \geq 0$. Possible orbit types: EO, TEO, CO, BO, COBO, MBO, COEO.

Region IV: all six zeros of $\tilde{R}$ are real and $\tilde{R}(\tilde{r}) \geq 0$. Possible orbit types: EO, TEO, CO, BO, COBO, MBO, COEO.

From the condition of double zero, we can plot parametric $\tilde{L} - E^2$ diagrams; see, for example, in Figure 4. The polynomial $\tilde{R}$ has two positive zeros in the left region IIa, one negative and one positive zero in the right region IIa, four positive zeros in left region IIIa, three positive and one negative zeros in right region IIIa for the left figure, and for the right figure, there are no zeros in region Ib, one negative and one positive zero in region IIa, two negative zeros in region IIb, four positive zeros in the left region IIIa, three positive and one negative zeros in the right region IIIa. In regions marked with the letter "a", the orbits cross $\theta = \pi/2$ but not $\tilde{r} = 0$, whereas in regions marked with the letter "b", $\tilde{r} = 0$ can be crossed but $\theta = \pi/2$ is never crossed. The θ equation dose not allow geodesic motion in the grey areas. The $\tilde{L} - E^2$ diagrams for Kerr, Kerr–AdS$_4$, and Kerr–dilaton spacetime are also presented for compariso; there are four positive zeros on the left side of the vertical line, while there are three positive and one negative zeros on the other side in region IIIa.

As shown in [6], a non-vanishing cosmological constant can dramatically change the possible structure of orbits and the $\tilde{L} - E^2$ diagram. See, for example, the following: compared with the $\Lambda = 0$ case, the region in $\tilde{L} - E^2$ with four real zeros of $\tilde{R}(\tilde{r})$ becomes larger for $\Lambda < 0$, and the transit orbit in region where $\tilde{R}(\tilde{r})$ has no real zero is transformed to a bound orbit in the region where $\tilde{R}(\tilde{r})$ has two real zeros for $\Lambda < 0$. However, these might not necessarily be the cases here, because parameter b will affect the evolution of $\tilde{R}(\tilde{r})$. See in Figures 3 and 4 that region III becomes lager when parameter $\tilde{b}$ is nonzero, while a vertical line switch from $\lim_{\tilde{r}\to\infty}\tilde{R}(\tilde{r}) = \infty$ to $\lim_{\tilde{r}\to\infty}\tilde{R}(\tilde{r}) = -\infty$ appears when the cosmological constant is nonzero.

We observe from the discussions above that the parameter b will result in rich and complex orbital types compared to the case of Kerr–AdS$_4$ [6]. To be more specific about this point, we consider an interesting case: $\tilde{r} = 0$ as a double zero of $\tilde{R}$. From $\tilde{R}(0) = 0$ yields

$$\tilde{a} = 0, \quad \text{or} \quad \tilde{K} = \left(\tilde{a}E - \tilde{L}\Xi\right)^2. \tag{50}$$

From $\frac{d\tilde{R}}{d\tilde{r}}(0) = 0$, we have

$$\tilde{b} = 1, \quad \text{or} \quad \tilde{b} = \frac{\left(E\tilde{a} - \tilde{L}\Xi\right)^2 \tilde{l}^2}{E^2\tilde{a}^4 - E^2\tilde{a}^2\tilde{l}^2 - 2\,E\tilde{L}\Xi\tilde{a}^3 + \tilde{L}^2\Xi^2\tilde{a}^2 + \tilde{L}^2\Xi^2\tilde{l}^2 + \tilde{a}^2\tilde{l}^2}. \tag{51}$$

We find that $\tilde{r} = 0$ is not a double zero of $\tilde{R}$ in the case of Kerr–AdS$_4$ with $\tilde{a} = 0$ [6], but it is a double zero of $\tilde{R}$ in the case of Kerr–Sen–AdS$_4$ with $\tilde{a} = 0$ and $\tilde{b} = 1$. If $E\tilde{a} = \tilde{L}\Xi$, then $\tilde{r} = 0$ is a double zero of $\tilde{R}$ for both the case of Kerr–AdS$_4$ [6] and the case of Kerr–Sen–AdS$_4$ with $\tilde{b} = 0$. If $E\tilde{a} \neq \tilde{L}\Xi$ ($\tilde{b} \neq 0$), $\tilde{r} = 0$ is a double zero of $\tilde{R}$ only for the case of Kerr-Sen-AdS$_4$.

In Figure 5, we show the effective potential together with examples of energies for different orbit types. The green and blue curves represent the two branches of the effective potential. The red dots, which are the turning points of the orbits, denote the zeros of the polynomial $\tilde{R}(\tilde{r})$. The red dashed lines in the grey area correspond to energies. Since $\tilde{R}(\tilde{r}) < 0$, no motion is possible in the grey area. The θ equation does not allow geodesic motion ($\tilde{\Theta} < 0$) in the oblique lines area.

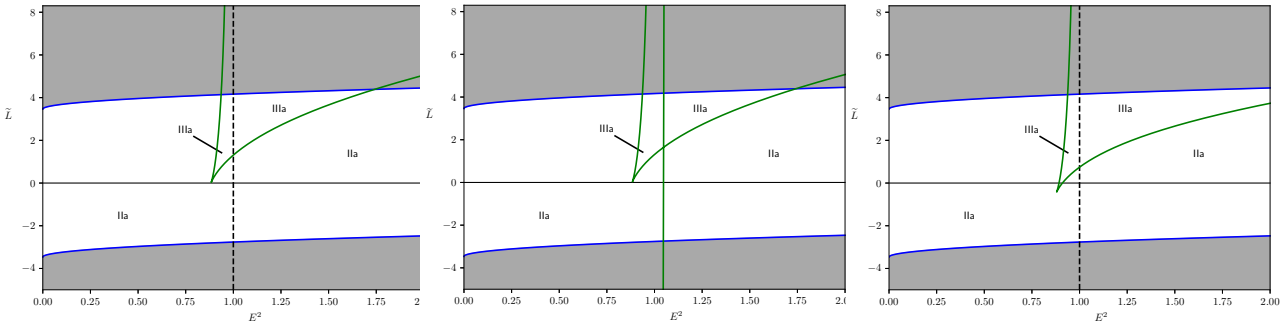

Figure 3. Combined $\tilde{L} - E^2$ diagrams of the $\tilde{r}$ motion (green lines) and θ motion (blue lines) with $\tilde{a} = 0.7$, $\tilde{K} = 12$, and $\tilde{b} = 0$, $\tilde{l}^2 = \infty$ in left column; $\tilde{b} = 0$, $\tilde{l}^2 = 3 \times 10^5$ in middle column; $\tilde{b} = 0.175$, $\tilde{l}^2 = \infty$ in right colum. In regions marked with "a", the orbits cross $\theta = \pi/2$ but not $\tilde{r} = 0$. The θ equation does not allow geodesic motion in the grey areas.

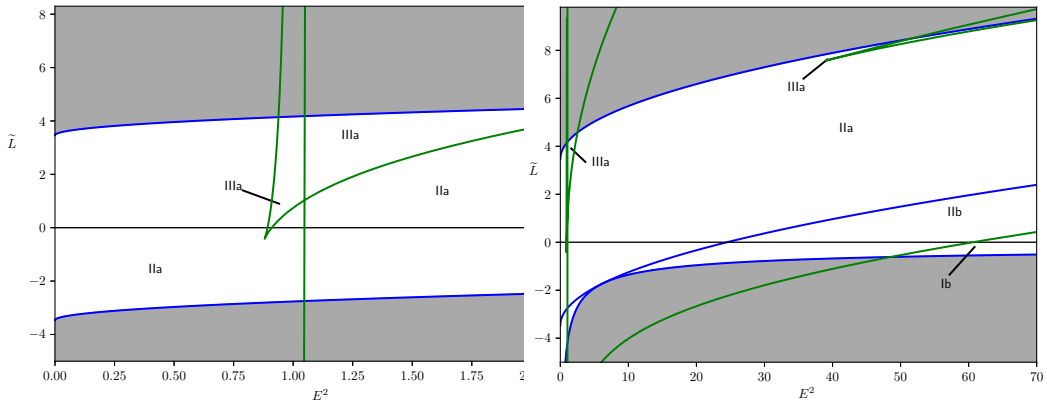

Figure 4. Combined $\tilde{L} - E^2$ diagrams of the $\tilde{r}$ motion (green lines) and θ motion (blue lines) with $\tilde{a} = 0.7$, $\tilde{K} = 12$, $\tilde{b} = 0.175$, $\tilde{l}^2 = 3 \times 10^5$. In regions marked with "b", $\tilde{r} = 0$ can be crossed but $\theta = \pi/2$ is never crossed.

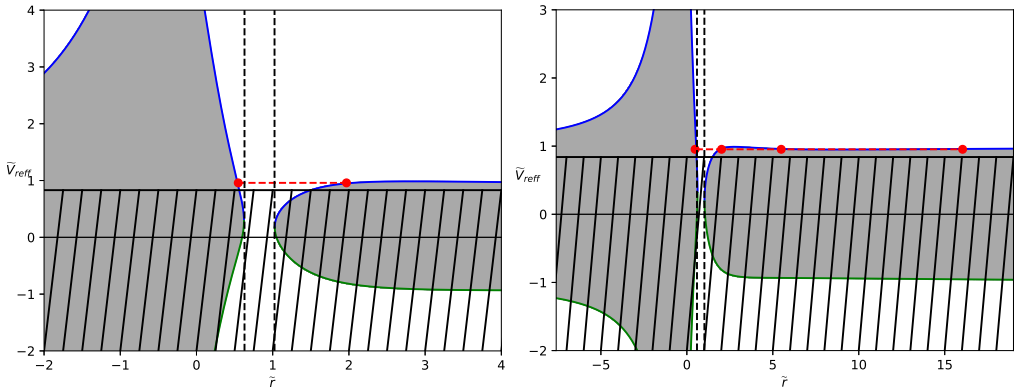

Figure 5. Plots of the effective potential: $\tilde{a} = 0.8$, $\tilde{K} = 12$, $\tilde{b} = 0.175$, $\tilde{l}^2 = \frac{1}{3} \times 10^{-5}$, $\tilde{L} = 0.45$ (for left column), and $\tilde{L} = 0.5$ (for right column). The blue and green curves show the two branches of the effective potential. The red dashed lines correspond to energies. The red dots mark the zeros of the polynomial R. No motion is possible in the grey area. No θ geodesic motions are allowed in the dashed oblique lines area. The vertical black dashed lines represent the position of the horizons.

5.2. Circular Orbits and Equatorial Circular Orbits

For the circular orbits (COs), we have the conditions: $\tilde{R}(\tilde{r}) = 0$ and $\mathrm{d}\tilde{R}(\tilde{r})/\mathrm{d}\tilde{r} = 0$; namely, $r_{\rm co}$ is a double root of $\tilde{R}(\tilde{r})$. If a double root of $\tilde{R}(\tilde{r})$ locates at the horizon, the orbits will be confined at this horizon. Stable circular orbits with $\tilde{r}_0$ occur if radial coordinates adjacent to $\tilde{r}_0$ are not allowed due to $R(\tilde{r})$, which happens if $\tilde{r}_0$ is a maximum of R; namely, the orbit is radially (vertically) stable (unstable) if $\partial^2_{\tilde{r}} \tilde{V}_{reff} \leq 0$ ($\partial^2_{\tilde{r}} \tilde{V}_{reff} > 0$). Because the expression of this inequality is very complex, we cannot provide an analytical solution; however, we can give some numerical solutions. Taking $\tilde{a} = 0.7$, $\tilde{L} = 0.5$, $\tilde{b} = 0.1$, $\tilde{l} = \infty$, and $\tilde{K} = 12$, the double zero conditions give $r_{\rm co} = 0.96$, and the inequality $\partial^2_{\tilde{r}} \tilde{V}_{reff} \leq 0$ gives $\tilde{r} < -0.8$, $-0.75 < \tilde{r} < 0.33$, $1.45 < \tilde{r} < 4.32$, $6.16 < \tilde{r} < 9.76$, and $\tilde{r} > 13.51$. So, the CO in this case is unstable.

The equatorial circular orbit (ECO) is a type of circular obit which lies in the equatorial plane. The angular velocity for particles is defined as: $\Omega = \dot{\varphi}/\dot{t}$. For circular orbits in the equatorial plane, $\dot{r} = \dot{\theta} = \ddot{r} = 0$ (equivalently $V_{reff} = 0$ and $V_{reff,r} = 0$, $r_{\rm eco}$ is the double root of $R(r)$); we have from Equation (8)

$$\begin{aligned}\Omega &= \frac{-\partial_r g_{t\varphi} \pm \sqrt{\left(\partial_r g_{t\varphi}\right)^2 - \left(\partial_r g_{tt}\right)\left(\partial_r g_{\varphi\varphi}\right)}}{\partial_r g_{\varphi\varphi}} \\ &= \frac{\rho^2\left(a^2 - l^2\right)^2\left[\frac{2a\left((b+r)\left(a^2+2r(2b+r)\right)-l^2M\right)}{\rho^2\left(a^2-l^2\right)} \pm 2\sqrt{\frac{l^2(b+r)(a^2(b+r)(2r(2b+r)+l^2)+2r(2b+r)(r(4b^2+l^2)+l^2(b-M)+6br^2+2r^3))}{\rho^4\left(a^2-l^2\right)^2}}\right]}{2l^2\left[-a^4(b+r)+a^2(r(l^2-4b^2)+l^2(b+M)-6br^2-2r^3)+2l^2r(b+r)(2b+r)\right]},\end{aligned} \tag{52}$$

where the $+/-$ sign refers to corotating/counterrotating orbits, namely orbits with angular momentum parallel (antiparallel) to the spin of the central object. In this case, the energy E and the angular momentum L, respectively, take the form

$$E = -\left(g_{tt} + \Omega g_{t\varphi}\right)\dot{t} \tag{53}$$

$$= \frac{\Delta_r\left[a^2 + l^2(a\Omega - 1)\right] - a\Delta_\theta\left[a^3 + a^2\Omega l^2 - al^2 + \Omega l^2 r(2b + r)\right]}{\rho\sqrt{\Delta_r\left(a^2 + l^2(a\Omega - 1)\right)^2 - \Delta_\theta\left(a^3 + a^2\Omega l^2 - al^2 + \Omega l^2 r(2b + r)\right)^2}}, \tag{54}$$

$$L = \left(g_{t\varphi} + \Omega g_{\varphi\varphi}\right)\dot{t} \tag{55}$$

$$= \frac{l^2\left[\Delta_\theta\left(a^2 + r(2b + r)\right)\left(a^3 + a^2\Omega l^2 - al^2 + \Omega l^2 r(2b + r)\right) - a\Delta_r\left(a^2 + l^2(a\Omega - 1)\right)\right]}{\rho^2(a - l)^2(a + l)^2\sqrt{\frac{\Delta_r\left(a^2+l^2(a\Omega-1)\right)^2-\Delta_\theta\left(a^3+a^2\Omega l^2-al^2+\Omega l^2 r(2b+r)\right)^2}{\rho^2(a-l)^2(a+l)^2}}}. \tag{56}$$

In terms of dimensionless quantity, the angular velocity Ω, the energy E, and the angular momentum L can be expressed as

$$\Omega = \frac{\tilde{\rho}^2\left(\tilde{a}^2-\tilde{l}^2\right)^2\left[\frac{2\tilde{a}\left(\left(\tilde{b}+\tilde{r}\right)\left(\tilde{a}^2+2\tilde{r}\left(2\tilde{b}+\tilde{r}\right)\right)-\tilde{l}^2\right)}{\tilde{\rho}^2\left(\tilde{a}^2-\tilde{l}^2\right)} \pm 2\sqrt{\frac{\tilde{l}^2\left(\tilde{b}+\tilde{r}\right)\left(\tilde{a}^2\left(\tilde{b}+\tilde{r}\right)\left(2\tilde{r}\left(2\tilde{b}+\tilde{r}\right)+\tilde{l}^2\right)+2\tilde{r}\left(2\tilde{b}+\tilde{r}\right)\left(\tilde{l}^2\left(\tilde{b}+\tilde{r}-1\right)+2\tilde{r}\left(\tilde{b}+\tilde{r}\right)\left(2\tilde{b}+\tilde{r}\right)\right)\right)}{\tilde{\rho}^4\left(\tilde{a}^2-\tilde{l}^2\right)^2}}\right]}{2\tilde{l}^2\left[\tilde{a}^2\left(\tilde{l}^2\left(\tilde{b}+\tilde{r}+1\right)-2\tilde{r}\left(\tilde{b}+\tilde{r}\right)\left(2\tilde{b}+\tilde{r}\right)\right)-\tilde{a}^4\left(\tilde{b}+\tilde{r}\right)+2\tilde{l}^2\tilde{r}\left(\tilde{b}+\tilde{r}\right)\left(2\tilde{b}+\tilde{r}\right)\right]} \tag{57}$$

$$E = \frac{\Delta_{\tilde{r}}\left[\tilde{l}^2(\Omega\tilde{a}-1)+\tilde{a}^2\right]-\tilde{a}\left[\Omega\tilde{a}^2\tilde{l}^2-\tilde{a}\tilde{l}^2+\tilde{a}^3+\Omega\tilde{l}^2\tilde{r}\left(2\tilde{b}+\tilde{r}\right)\right]}{\tilde{\rho}^2\left(\tilde{a}^2-\tilde{l}^2\right)\sqrt{\frac{\Delta_{\tilde{r}}\left[\tilde{l}^2(\Omega\tilde{a}-1)+\tilde{a}^2\right]^2-\left[\Omega\tilde{a}^2\tilde{l}^2-\tilde{a}\tilde{l}^2+\tilde{a}^3+\Omega\tilde{l}^2\tilde{r}\left(2\tilde{b}+\tilde{r}\right)\right]^2}{\tilde{\rho}^2\left(\tilde{a}^2-\tilde{l}^2\right)^2}}}, \tag{58}$$

$$L = \frac{\tilde{l}^2\left[\left(\tilde{a}^2+\tilde{r}\left(2\tilde{b}+\tilde{r}\right)\right)\left(\Omega\tilde{a}^2\tilde{l}^2-\tilde{a}\tilde{l}^2+\tilde{a}^3+\Omega\tilde{l}^2\tilde{r}\left(2\tilde{b}+\tilde{r}\right)\right)-\tilde{a}\Delta_{\tilde{r}}\left(\tilde{l}^2(\Omega\tilde{a}-1)+\tilde{a}^2\right)\right]}{\tilde{\rho}^2\left(\tilde{a}^2-\tilde{l}^2\right)^2\sqrt{\frac{\Delta_{\tilde{r}}\left[\tilde{l}^2(\Omega\tilde{a}-1)+\tilde{a}^2\right]^2-\left[\Omega\tilde{a}^2\tilde{l}^2-\tilde{a}\tilde{l}^2+\tilde{a}^3+\Omega\tilde{l}^2\tilde{r}\left(2\tilde{b}+\tilde{r}\right)\right]^2}{\tilde{\rho}^2\left(\tilde{a}^2-\tilde{l}^2\right)^2}}}. \tag{59}$$

Radial profiles of the functions $E_{+/-}(\tilde{r})$ ($F_{+/-}$ denote that Ω takes $+$ in F_+ or $-$ in F_-) for $\tilde{a} = 0.8$, and various values of other parameters are shown in the Figure 6. The evolutions of $E_{+/-}$ for large $\tilde{r}$ tend to be consistent for particles circling around a Kerr ($\tilde{l} = \infty$ and $\tilde{b} = 0$) or a Kerr-dilation black hole ($\tilde{l} = \infty$ and $\tilde{b} \neq 0$) or a Kerr–Sen–AdS$_4$ ($\tilde{l} \neq \infty$ and $\tilde{b} \neq 0$), but the differences in $E_{+/-}$ in Kerr–AdS$_4$ ($\tilde{l} \neq \infty$ and $\tilde{b} = 0$) spacetime and in the other three spacetimes are obvious. For small $\tilde{r}$, the evolutions of E_+ in Kerr and Kerr–AdS$_4$ spacetime tend to be consistent, while they are distinguished from those in Kerr-dilation and Kerr–Sen–AdS$_4$ spacetime; E_- tends to be consistent in these four spacetimes.

Radial profiles of the functions $L_{+/-}(\tilde{r})$ for $\tilde{a} = 0.8$ and various values of other parameters are shown in the Figure 7. The evolutions of L_+ for large $\tilde{r}$ tend to be consistent for particles circling around a Kerr or a Kerr-dilation black hole ($\tilde{l} = \infty$ and $\tilde{b} \neq 0$), but the differences in L_+ in Kerr–AdS$_4$ spacetime and in Kerr–Sen–AdS$_4$ spacetime are large, indicating that the parameter $\tilde{b}$ has a significant impact on L_+. For small $\tilde{r}$, the evolutions of L_+ in Kerr and Kerr–AdS$_4$ spacetime also tend to be consistent, while they are distinguished from those in Kerr-dilation and Kerr–Sen–AdS$_4$ spacetime. L_- is positive in Kerr–Sen–AdS$_4$ spacetime, while it is negative in the other three spacetimes.

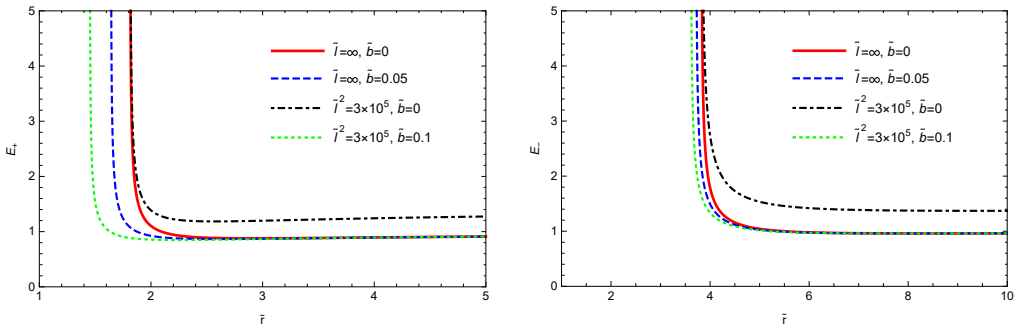

Figure 6. Radial profiles of the functions $E_{+/-}(\tilde{r})$ for equatorial circular orbits with $\tilde{a} = 0.8$ and various values of other parameters.

5.3. Innermost Stable Circular Orbit

For a test particle in the gravitational potential of a central body, the innermost stable circular orbit (ISCO) is of importance as it represents the transition from stable orbit to those which fall through the event horizon. The ISCO is given by the conditions:

$$R(\tilde{r}) = 0, \quad \frac{dR}{d\tilde{r}} = 0, \quad \frac{d^2R}{d\tilde{r}^2} = 0, \tag{60}$$

or equivalently $\dot{\tilde{r}} = \ddot{\tilde{r}} = \dddot{\tilde{r}} = 0$. Namely, $\tilde{r}_{\rm ISCO}$ is the triple root of $R(\tilde{r})$. Since $\partial_{\tilde{r}}^2 \tilde{V}_{reff} = 0$, the ISCOs are marginally stable orbits around the black hole.

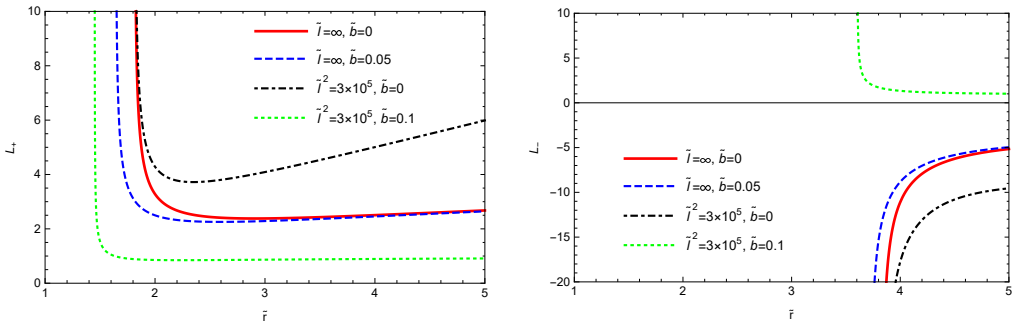

Figure 7. Radial profiles of the functions $L_{+/-}(\tilde{r})$ for equatorial circular orbits with $\tilde{a} = 0.8$ and various values of other parameters.

In Figure 8, we plot $E^2 - \tilde{r}$ and $\tilde{L} - \tilde{r}$ diagrams for some ISCOs in Kerr, Kerr-dilaton, Kerr–AdS$_4$, and Kerr–Sen–AdS$_4$ spacetimes. We observe that E^2 decreases as $\tilde{r}$ increases, while $\tilde{L}$ decreases to some minimum value and then behaves as a monotonous function. For large $\tilde{r}$, both E^2 and $\tilde{L}$ for there ISCOs run to the same values. But for small $\tilde{r}$, parameter b will bring significant differences to E^2 and $\tilde{L}$.

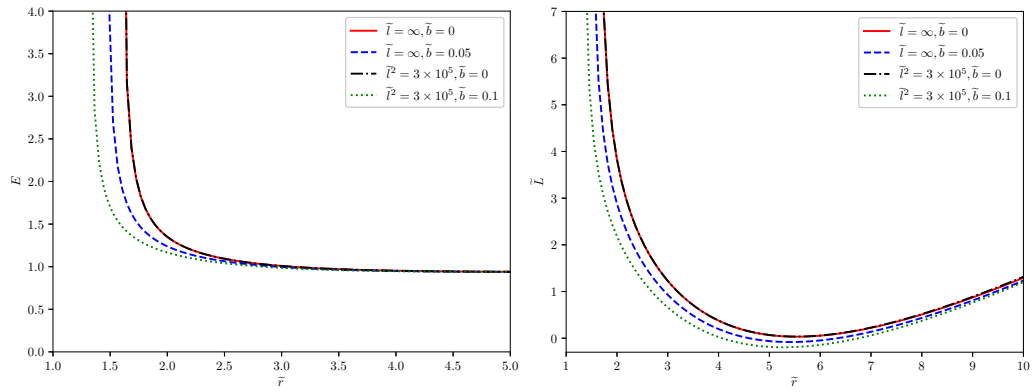

Figure 8. $E^2 - \tilde{r}$ and $\tilde{L} - \tilde{r}$ diagrams for some ISCOs with some special values of parameters.

6. Conclusions

In this paper, we have discussed the motion of particles in the Kerr–Sen–AdS$_4$ spacetime. We have obtained the geodesic equations. Using parametric diagrams, we have shown some regions where the $\tilde{r}$ and the θ geodesic motions are allowed. We have analyzed in detail the impact of parameter related to dilatonic scalar on the orbit and found that it will result in more rich and complex orbit types; see that, for example, $\tilde{r} = 0$ is not a double zero of $\tilde{R}$ in the case of Kerr–AdS$_4$ with $\tilde{a} = 0$ [6], but it is a double zero of $\tilde{R}$ in the case of Kerr–Sen–AdS$_4$ with $\tilde{a} = 0$ and $\tilde{b} = 1$. We also have discussed how the parameters of the model affect the equatorial circular orbit and the innermost stable circular orbit and visualize the energies and angular momentums of particles with diagrams. Other topics, such as the bound on the Carter constant, the angular motion for null/time-like geodesics, the radial motion for null/time-like geodesics, and geodesic motion in naked singularity spacetime (2), we leave for future studies.

Author Contributions: Conceptualization, R.-J.Y.; Methodology, Z.-W.H. and R.-J.Y.; Formal analysis, Z.C., M.L. and R.-J.Y.; Investigation, R.-J.Y.; Resources, R.-J.Y.; Data curation, Z.C., M.L., W.-Q.W., T.-Y.H. and R.-J.Y.; Writing—original draft, Z.C. and R.-J.Y.; Writing—review & editing, R.-J.Y.; Visualization, Z.C., M.L., W.-Q.W., T.-Y.H. and R.-J.Y.; Supervision, Z.-W.H. and R.-J.Y.; Project administration, R.-J.Y.; Funding acquisition, R.-J.Y. All authors have read and agreed to the published version of the manuscript.

Funding: This study is supported in part by the National Natural Science Foundation of China (Grant No. 12333008) and the Hebei Provincial Natural Science Foundation of China (Grant No. A2021201034).

Data Availability Statement: Data are contained within the article.

Conflicts of Interest: The authors declare no conflict of interest.

References

1. Hagihara, Y. Theory of the relativistic trajeetories in a gravitational field of schwarzschild. *Jpn. J. Astron. Geophys.* **1930**, *8*, 67.
2. Chandrasekhar, S. *The Mathematical Theory of Black Holes*; Oxford University Press: Oxford, UK, 1983.
3. Hoseini, B.; Saffari, R.; Soroushfar, S. Study of the geodesic equations of a spherical symmetric spacetime in conformal Weyl gravity. *Class. Quant. Grav.* **2017**, *34*, 055004. [CrossRef]
4. Soroushfar, S.; Saffari, R.; Kazempour, S.; Grunau, S.; Kunz, J. Detailed study of geodesics in the Kerr-Newman-(A)dS spacetime and the rotating charged black hole spacetime in $f(R)$ gravity. *Phys. Rev. D* **2016**, *94*, 024052. [CrossRef]
5. Hackmann, E.; Lammerzahl, C. Complete Analytic Solution of the Geodesic Equation in Schwarzschild-(Anti-)de Sitter Spacetimes. *Phys. Rev. Lett.* **2008**, *100*, 171101. [CrossRef] [PubMed]
6. Hackmann, E.; Lammerzahl, C.; Kagramanova, V.; Kunz, J. Analytical solution of the geodesic equation in Kerr-(anti) de Sitter space-times. *Phys. Rev. D* **2010**, *81*, 044020. [CrossRef]
7. Soroushfar, S.; Saffari, R.; Kunz, J.; Lämmerzahl, C. Analytical solutions of the geodesic equation in the spacetime of a black hole in f(R) gravity. *Phys. Rev. D* **2015**, *92*, 044010. [CrossRef]
8. Flathmann, K.; Grunau, S. Analytic solutions of the geodesic equation for Einstein-Maxwell-dilaton-axion black holes. *Phys. Rev. D* **2015**, *92*, 104027.
9. Soroushfar, S.; Saffari, R.; Sahami, E. Geodesic equations in the static and rotating dilaton black holes: Analytical solutions and applications. *Phys. Rev. D* **2016**, *94*, 024010. [CrossRef]
10. Flathmann, K.; Grunau, S. Analytic solutions of the geodesic equation for $U(1)^2$ dyonic rotating black holes. *Phys. Rev. D* **2016**, *94*, 124013. [CrossRef]
11. Hackmann, E.; Kagramanova, V.; Kunz, J.; Lammerzahl, C. Analytic solutions of the geodesic equation in higher dimensional static spherically symmetric space-times. *Phys. Rev. D* **2008**, *78*, 124018. [CrossRef]
12. Kagramanova, V.; Reimers, S. Analytic treatment of geodesics in five-dimensional Myers-Perry space–times. *Phys. Rev. D* **2012**, *86*, 084029. [CrossRef]
13. Diemer, V.; Kunz, J. Supersymmetric rotating black hole spacetime tested by geodesics. *Phys. Rev. D* **2014**, *89*, 084001. [CrossRef]
14. Diemer, V.; Kunz, J.; Lämmerzahl, C.; Reimers, S. Dynamics of test particles in the general five-dimensional Myers-Perry spacetime. *Phys. Rev. D* **2014**, *89*, 124026. [CrossRef]
15. Kagramanova, V.; Kunz, J.; Hackmann, E.; Lammerzahl, C. Analytic treatment of complete and incomplete geodesics in Taub-NUT space-times. *Phys. Rev. D* **2010**, *81*, 124044. [CrossRef]
16. Diemer, V.; Smolarek, E. Dynamics of test particles in thin-shell wormhole spacetimes. *Class. Quant. Grav.* **2013**, *30*, 175014. [CrossRef]
17. Hackmann, E.; Lammerzahl, C. Geodesic equation in Schwarzschild- (anti-) de Sitter space-times: Analytical solutions and applications. *Phys. Rev. D* **2008**, *78*, 024035. [CrossRef]
18. Hackmann, E.; Kagramanova, V.; Kunz, J.; Lammerzahl, C. Analytic solutions of the geodesic equation in axially symmetric space-times. *Europhys. Lett.* **2009**, *88*, 30008. [CrossRef]
19. Grunau, S.; Kagramanova, V. Geodesics of electrically and magnetically charged test particles in the Reissner-Nordström space-time: Analytical solutions. *Phys. Rev. D* **2011**, *83*, 044009. [CrossRef]
20. Enolski, V.Z.; Hackmann, E.; Kagramanova, V.; Kunz, J.; Lammerzahl, C. Inversion of hyperelliptic integrals of arbitrary genus with application to particle motion in General Relativity. *J. Geom. Phys.* **2011**, *61*, 899–921. [CrossRef]
21. Hackmann, E.; Hartmann, B.; Lammerzahl, C.; Sirimachan, P. Test particle motion in the space-time of a Kerr black hole pierced by a cosmic string. *Phys. Rev. D* **2010**, *82*, 044024. [CrossRef]
22. Hackmann, E.; Hartmann, B.; Laemmerzahl, C.; Sirimachan, P. The Complete set of solutions of the geodesic equations in the space-time of a Schwarzschild black hole pierced by a cosmic string. *Phys. Rev. D* **2010**, *81*, 064016. [CrossRef]
23. Grunau, S.; Khamesra, B. Geodesic motion in the (rotating) black string spacetime. *Phys. Rev. D* **2013**, *87*, 124019. [CrossRef]
24. Ozdemir, F.; Ozdemir, N.; Kaynak, B.T. Multi-black holes solution with cosmic strings. *Int. J. Mod. Phys. A* **2004**, *19*, 1549–1557. [CrossRef]
25. Aliev, A.N.; Galtsov, D.V. Gravitational Effects in the Field of a Central Body Threaded by a Cosmic String. *Sov. Astron. Lett.* **1988**, *14*, 48.
26. Galtsov, D.V.; Masar, E. Geodesics in Space-times Containing Cosmic Strings. *Class. Quant. Grav.* **1989**, *6*, 1313–1341. [CrossRef]
27. Chakraborty, S.; Biswas, L. Motion of test particles in the gravitational field of cosmic strings in different situations. *Class. Quant. Grav.* **1996**, *13*, 2153–2161. [CrossRef]
28. Compère, G.; Liu, Y.; Long, J. Classification of radial Kerr geodesic motion. *Phys. Rev. D* **2022**, *105*, 024075. [CrossRef]

29. Cieślik, A.; Hackmann, E.; Mach, P. Kerr geodesics in terms of Weierstrass elliptic functions. *Phys. Rev. D* **2023**, *108*, 024056. [CrossRef]
30. Kraniotis, G.V. Precise relativistic orbits in Kerr space-time with a cosmological constant. *Class. Quant. Grav.* **2004**, *21*, 4743–4769. [CrossRef]
31. Kraniotis, G.V. Gravitational redshift/blueshift of light emitted by geodesic test particles, frame-dragging and pericentre-shift effects, in the Kerr–Newman–de Sitter and Kerr–Newman black hole geometries. *Eur. Phys. J. C* **2021**, *81*, 147. [CrossRef]
32. García, A.; Hackmann, E.; Kunz, J.; Lämmerzahl, C.; Macías, A. Motion of test particles in a regular black hole space–time. *J. Math. Phys.* **2015**, *56*, 032501. [CrossRef]
33. Yang, Y.; Zhang, X. Geodesics on metrics of Eguchi–Hanson type. *Eur. Phys. J. C* **2023**, *83*, 574. [CrossRef]
34. Deng, X.M. Geodesics and periodic orbits around quantum-corrected black holes. *Phys. Dark Univ.* **2020**, *30*, 100629. [CrossRef]
35. Wei, S.W.; Yang, J.; Liu, Y.X. Geodesics and periodic orbits in Kehagias-Sfetsos black holes in deformed Horava-Lifshitz gravity. *Phys. Rev. D* **2019**, *99*, 104016. [CrossRef]
36. Fathi, M.; Olivares, M.; Villanueva, J.R. Study of null and time-like geodesics in the exterior of a Schwarzschild black hole with quintessence and cloud of strings. *Eur. Phys. J. C* **2022**, *82*, 629. [CrossRef]
37. Ospino, J.; Hernandez-Pastora, J.L.; Nunez, L.A. All analytic solutions for geodesic motion in axially symmetric space-times. *Eur. Phys. J. C* **2022**, *82*, 591; Erratum in *Eur. Phys. J. C* **2022**, *82*, 627. [CrossRef]
38. Liu, Y.; Sun, B. The Analytical Solutions of Equatorial Geodesic Motion in Kerr Spacetime. *arXiv* **2023**, arXiv:2305.11045.
39. Wang, C.Y.; Lee, D.S.; Lin, C.Y. Null and timelike geodesics in the Kerr-Newman black hole exterior. *Phys. Rev. D* **2022**, *106*, 084048. [CrossRef]
40. Mummery, A.; Balbus, S. Complete characterization of the orbital shapes of the noncircular Kerr geodesic solutions with circular orbit constants of motion. *Phys. Rev. D* **2023**, *107*, 124058. [CrossRef]
41. Frolov, V.P.; Krtous, P.; Kubiznak, D. Black holes, hidden symmetries, and complete integrability. *Living Rev. Rel.* **2017**, *20*, 6. [CrossRef]
42. Okai, T. Global structure and thermodynamic property of the four-dimensional twisted Kerr solution. *Prog. Theor. Phys.* **1994**, *92*, 47–66. [CrossRef]
43. Wu, S.Q.; Cai, X. Massive complex scalar field in the Kerr-Sen geometry: Exact solution of wave equation and Hawking radiation. *J. Math. Phys.* **2003**, *44*, 1084–1088. [CrossRef]
44. Hioki, K.; Miyamoto, U. Hidden symmetries, null geodesics, and photon capture in the Sen black hole. *Phys. Rev. D* **2008**, *78*, 044007. [CrossRef]
45. Blaga, P.A.; Blaga, C. Bounded radial geodesics around a Kerr-Sen black hole. *Class. Quant. Grav.* **2001**, *18*, 3893–3905. [CrossRef]
46. Houri, T.; Kubiznak, D.; Warnick, C.M.; Yasui, Y. Generalized hidden symmetries and the Kerr-Sen black hole. *J. High Energy Phys.* **2010**, *07*, 055. [CrossRef]
47. Wu, D.; Wu, P.; Yu, H.; Wu, S.Q. Are ultraspinning Kerr-Sen- AdS_4 black holes always superentropic? *Phys. Rev. D* **2020**, *102*, 044007. [CrossRef]
48. Plebanski, J.F.; Demianski, M. Rotating, charged, and uniformly accelerating mass in general relativity. *Annals Phys.* **1976**, *98*, 98–127. [CrossRef]
49. Carter, B. Hamilton-Jacobi and Schrodinger separable solutions of Einstein's equations. *Commun. Math. Phys.* **1968**, *10*, 280–310. [CrossRef]
50. Sen, A. Rotating charged black hole solution in heterotic string theory. *Phys. Rev. Lett.* **1992**, *69*, 1006–1009. [CrossRef]
51. Carter, B. Global structure of the Kerr family of gravitational fields. *Phys. Rev.* **1968**, *174*, 1559–1571. [CrossRef]
52. Wilkins, D.C. Bound Geodesics in the Kerr Metric. *Phys. Rev. D* **1972**, *5*, 814–822. [CrossRef]
53. Mino, Y. Perturbative approach to an orbital evolution around a supermassive black hole. *Phys. Rev. D* **2003**, *67*, 084027. [CrossRef]